ChemInform Abstract: Synthetic Approaches for Noncentrosymmetric Molybdates

ARTICLE *in* INORGANIC CHEMISTRY · NOVEMBER 2008

Impact Factor: 4.76 · DOI: 10.1021/ic800572g · Source: PubMed

5 AUTHORS, INCLUDING:

Alexander J Norquist

Haverford College

96 PUBLICATIONS **2,140** CITATIONS

SEE PROFILE

Inorg. Chem. **2008**, *47*, 8518−8525

Forum

Synthetic Approaches for Noncentrosymmetric Molybdates

Desmond J. Hubbard,[†] Alexander R. Johnston,[†] Hernan Sanchez Casalongue,[†] Amy Narducci Sarjeant,[‡] and Alexander J. Norquist*[,†]

Department of Chemistry, Johns Hopkins University, Baltimore, Maryland 21218, and Department of Chemistry, Haverford College, Haverford, Pennsylvania 19041

Received March 31, 2008

The use of second-order Jahn−Teller active Mo^{VI} centers and chiral organic amines is discussed as an approach to crystallographic noncentrosymmetry. Several series of reactions, conducted under mild hydrothermal conditions, were designed to probe important reaction variables. Correlations between reagent and solvent concentrations and the molybdate structure were investigated using composition space analysis, which allows for the isolation of specific reaction variables. The effects of amine structure variation were probed using multiple series of related amines, which consisted of either linear diamines or ethylenediamine derivatives. The addition of fluoride results in the loss of amine-based structural variations. Chiral organic amines were used to demonstrate the viability of using such components to control the three-dimensional symmetry in new materials. The synthesis, structure, and characterization of eight new organically templated polyoxomolybdates and polyoxofluoromolybdates are reported.

Introduction

Materials that possess crystallographic noncentrosymmetry are of great interest to researchers because they can exhibit several desirable physical properties,[1] including nonlinear optical activity, such as second harmonic generation (SHG) and piezoelectricity. While the presence of these technologically advantageous properties is solely dependent upon symmetry,[2] the performance of specific compounds is determined by the structure and composition.

While the a priori synthesis of noncentrosymmetric materials is difficult, several approaches are currently employed. First, the incorporation of metal centers with acentric coordination environments in inorganic materials can be achieved through the use of second-order Jahn−Teller active cations, specifically d^0 transition metals.[3–5] Early transition metals are of specific interest owing to the high polarizabilities of the M−O bonds, the suspected source of the unusually high SHG responses in materials such as $KTiOPO_4$[6,7] and $LiNbO_3$.[2] In addition, main-group cations with nonbonded electron pairs (such as selenites,[8] tellurites,[9] and iodates[10]) and early-transition-metal oxide fluoride anions[11,12] also exhibit local acentric coordination environments and have been used in the preparation of new noncentrosymmetic materials. Second, the combination of acentric organic linkers and tetrahedral inorganic nodes in extended hybrid materials has been shown to promote crystallization in noncentrosymmetic space groups through the prohibition of intraframework inversion centers.[13,14] Third, the formation of mixed ionic and covalent sublattices has been

* To whom correspondence should be addressed. E-mail: anorquis@haverford.edu.
[†] Haverford College.
[‡] Johns Hopkins University.

(1) Halasyamani, P. S.; Poeppelmeier, K. R. *Chem. Mater.* **1998**, *10*, 2753–2769.
(2) Chen, C. T.; Liu, G. Z. *Annu. Rev. Mater. Sci.* **1986**, *16*, 203–243.
(3) Pearson, R. G. *J. Am. Chem. Soc.* **1969**, *91*, 4947–4955.
(4) Wheeler, R. A.; Whangbo, M. H.; Hughbanks, T.; Hoffmann, R.; Burdett, J. K.; Albright, T. A. *J. Am. Chem. Soc.* **1986**, *108*, 2222–2236.
(5) Kunz, M.; Brown, I. D. *J. Solid State Chem.* **1995**, *115*, 395–406.
(6) Jeggo, C. R.; Boyd, G. D. *J. Appl. Phys.* **1970**, *41*, 2741–2743.
(7) Levine, B. F. *Phys. Rev. B* **1973**, *7*, 2600–2626.
(8) Harrison, W. T. A.; Dussack, L. L.; Jacobson, A. J. *J. Solid State Chem.* **1996**, *125*, 234–242.
(9) Ok, K. M.; Halasyamani, P. S. *Chem. Mater.* **2002**, *14*, 2360–2364.
(10) Sykora, R. E.; Ok, K. M.; Halasyamani, P. S.; Wells, D. M.; Albrecht-Schmitt, T. E. *Chem. Mater.* **2002**, *14*, 2741–2749.
(11) Maggard, P. A.; Stern, C. L.; Poeppelmeier, K. R. *J. Am. Chem. Soc.* **2001**, *123*, 7742–7743.
(12) Marvel, M. R.; Lesage, J.; Baek, J.; Halasyamani, P. S.; Stern, C. L.; Poeppelmeier, K. R. *J. Am. Chem. Soc.* **2007**, *129*, 13963–13969.
(13) Evans Owen, R.; Lin, W. *Acc. Chem. Res.* **2002**, *35*, 511–522.
(14) Moulton, B.; Zaworotko, M. J. *Chem. Rev.* **2001**, *101*, 1629–1658.

10.1021/ic800572g CCC: $40.75
Published on Web 09/29/2008

achieved using salt-inclusion reactions.[15,16] Noncentrosymmetry in these compounds is promoted through cation ordering in the covalent lattices by salt lattice anions. Fourth, the extension of families of compounds that are known to often crystallize in noncentrosymmetric space groups is a viable approach to new functional materials. Notable examples include the targeted syntheses of novel tungsten bronzes[17] and borates.[18–20] Fifth, the inclusion of chiral components has been achieved through the use of specific coordination complexes,[21] amino acids,[22] and organic amines.[23–27] Great diversity in the form of these chiral components suggests broad applicability of this technique to a wide range of systems.

We have chosen to use a combination of approaches for the directed synthesis of new noncentrosymmetric materials. Specifically, the focus of our work is the inclusion of chiral organic amines in polyoxo compounds that contain second-order Jahn−Teller active Mo^{VI} centers. It is well-known that the SHG properties of a compound are largely based on the anionic component[28] and that the structural chemistry of polyoxomolybdates is exceptionally diverse.[29] To address these issues, we have conducted several series of experiments designed to probe the factors that govern the structure of the polyoxomolybdate component and to address the effects of both the amine structure and symmetry. The results of this work include the synthesis and characterization of a number of compounds that contain a range of polyoxomolybdates, whose structures range from zero-dimensional molecular anions to a two-dimensional extended layer. See Figures 1–3.

Experimental Section

Materials. $Na_2MoO_4 \cdot 2H_2O$ (99%), H_2SO_4 (98%), *N*,*N*′-diethylethylenediamine (deed, 95%), *N*,*N*-dimethyl-*N*′-ethylethylenediamine (dmeed, 98%), *N*,*N*,*N*′,*N*′-tetramethylethylenediamine (tmed, 99%), tris(2-aminoethyl)amine (tren, 95%), hydrochloric acid (37%), and KOH (85%) were purchased from Aldrich and used as received. Deionized water was used in these syntheses.

Synthesis. All reactions were conducted in 20 mL polypropylene screw-top bottles and adjusted to pH 5 by the addition of hydrochloric acid and aqueous 30% KOH. Reactions were heated to 100 °C in an oil bath and allowed to soak for 16 h. The reactions were then cooled in air, the bottles were opened, and the products were recovered through filtration. Powder X-ray diffraction patterns of each bulk sample match the pattern generated from the respective single-crystal X-ray structure data.

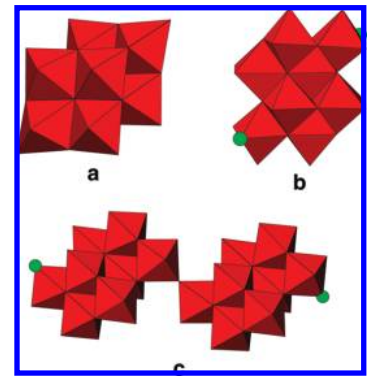

Figure 1. Polyhedral representations of (a) β-$[Mo_8O_{26}]^{4-}$, (b) $[Mo_8O_{26}F_2]^{6-}$, and (c) $[Mo_{16}O_{53}F_2]^{12-}$ molecular anions. Fluoride ligands are shown as green spheres.

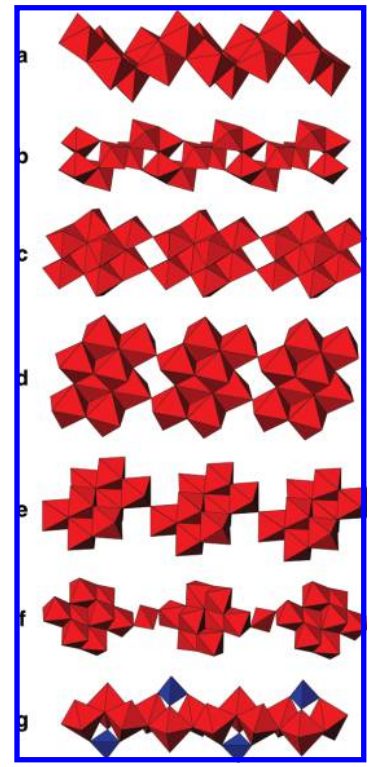

Figure 2. Polyhedral representations of (a) $[Mo_3O_{10}]_n^{2n-}$ type I, (b) $[Mo_3O_{10}]_n^{2n-}$ type II, (c) $[Mo_8O_{26}]_n^{4n-}$ type I, (d) $[Mo_8O_{26}]_n^{4n-}$ type II, (e) $[Mo_8O_{27}]_n^{6n-}$, (f) $[Mo_9O_{30}]_n^{6n-}$, and (g) $[(MoO_3)_3(SO_4)]_n^{2n-}$ chains. Red and blue polyhedra represent $[MoO_6]$ and $[SO_4]$, respectively.

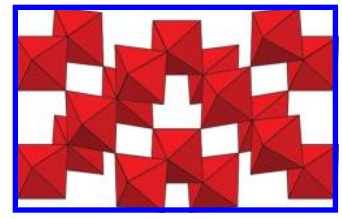

Figure 3. Polyhedral representation of $[Mo_5O_{16}]_n^{2n-}$ layers.

(15) Hwu, S.-J.; Ulutagay-Kartin, M.; Clayhold, J. A.; Mackay, R.; Wardojo, T. A.; O'Connor, C. J.; Krawiec, M. *J. Am. Chem. Soc.* **2002**, *124*, 12404–12405.
(16) Huang, Q.; Hwu, S.-J. *Inorg. Chem.* **2003**, *42*, 655–657.
(17) Chi, E. O.; Gandini, A.; Ok, K. M.; Zhang, L.; Halasyamani, P. S. *Chem. Mater.* **2004**, *16*, 3616–3622.
(18) Knyrim, J. S.; Becker, P.; Johrendt, D.; Huppertz, H. *Angew. Chem., Int. Ed.* **2006**, *45*, 8239–8241.
(19) Pan, S.; Wu, Y.; Fu, P.; Zhang, G.; Li, Z.; Du, C.; Chen, C. *Chem. Mater.* **2003**, *15*, 2218–2221.
(20) Chen, C.; Wang, Y.; Wu, B.; Wu, K.; Zeng, W.; Yu, L. *Nature* **1995**, *374*, 290.
(21) Kepert, C. J.; Prior, T. J.; Rosseinsky, M. J. *J. Am. Chem. Soc.* **2000**, *122*, 5158–5168.
(22) Inoue, M.; Yamase, T. *Bull. Chem. Soc. Jpn.* **1995**, *68*, 3055–3063.
(23) Nenoff, T. M.; Thoma, S. G.; Provencio, P.; Maxwell, R. S. *Chem. Mater.* **1998**, *10*, 3077–3080.
(24) Lin, H.-M.; Lii, K.-H. *Inorg. Chem.* **1998**, *37*, 4220–4222.
(25) Gutnick, J. R.; Muller, E. A.; Sarjeant, A. N.; Norquist, A. J. *Inorg. Chem.* **2004**, *43*, 6528–6530.
(26) Muller, E. A.; Cannon, R. J.; Sarjeant, A. N.; Ok, K. M.; Halasyamani, P. S.; Norquist, A. J. *Cryst. Growth Des.* **2005**, *5*, 1913–1917.
(27) Veltman, T. R.; Stover, A. K.; Sarjeant, A. N.; Ok, K. M.; Halasyamani, P. S.; Norquist, A. J. *Inorg. Chem.* **2006**, *45*, 5529–5537.
(28) Ye, N.; Chen, Q.; Wu, B.; Chen, C. *J. Appl. Phys.* **1998**, *84*, 555–558.
(29) Cruywagen, J. J. *Adv. Inorg. Chem.* **2000**, *49*, 127–182.

Compounds **1**−**4** were synthesized from reaction gels with approximate compositions of 1.5:1:100:1.25 $Na_2MoO_4 \cdot 2H_2O$:amine:H_2O:H_2SO_4. Compounds **5**−**8** were synthesized from reaction gels with approximate compositions of 1.5:1:100:1.25:*x* $Na_2MoO_4 \cdot 2H_2O$:amine:H_2O:H_2SO_4:KF, where *x* ranges between 0.2 and 0.8. Specific moles and masses for the synthesis of each compound are listed in the Supporting Information.

$[C_6H_{18}N_2]_2[Mo_8O_{26}] \cdot 2H_2O$ (1): colorless blocks. Elem microanal. Obsd (calcd) for **1**: C, 11.31 (9.89); H, 2.73 (2.75); N, 3.79 (3.85). IR data: N−H 3060, 1567 cm^{-1}, C−H 1458 cm^{-1}, Mo═O 910 cm^{-1}. **$[C_6H_{18}N_2]_2[Mo_8O_{26}]$ (2):** colorless plates. Elem microanal. Obsd (calcd) for **2**: C, 10.28 (10.41); H, 2.25 (2.54); N, 4.05 (3.94). IR data: N−H 3039, 1560 cm^{-1}, C−H 1463 cm^{-1}, Mo═O 951 cm^{-1}. **$[C_6H_{18}N_2]_2[Mo_8O_{26}]$ (3):** colorless rods. Elem microanal. Obsd (calcd) for **3**: C, 11.14 (10.14); H, 2.63 (2.54); N, 4.26 (3.98). IR data: N−H 3073 cm^{-1}, C−H 1460 cm^{-1}, Mo═O 925 cm^{-1}. **$[C_6H_{21}N_4]_2[Mo_8O_{27}] \cdot 2H_2O$ (4):** colorless blocks. Elem microanal. Obsd (calcd) for **4**: C, 10.37 (9.39); H, 3.44 (3.00); N, 7.74 (7.30). IR data: N−H 3114, 1591 cm^{-1}, C−H 1510 cm^{-1}, Mo═O 923 cm^{-1}. **$[C_6H_{18}N_2]_3[Mo_8O_{26}F_2] \cdot 4H_2O$ (5):** colorless rods. Elem microanal. Obsd (calcd) for **5**: C, 13.37 (13.09); H, 4.15 (3.88); N, 5.08 (5.09). IR data: N−H 3011, 1636 cm^{-1}, C−H 1458 cm^{-1}, Mo═O 930 cm^{-1}, Mo−F 485, 562 cm^{-1}. **$[C_6H_{18}N_2]_3[Mo_8O_{26}F_2] \cdot 5H_2O$ (6):** colorless rods. Elem microanal. Obsd (calcd) for **6**: C, 13.27 (13.05); H, 3.45 (3.24); N, 5.03 (5.07); F, 2.20 (2.30). IR data: N−H 3020, 1588 cm^{-1}, C−H 1468 cm^{-1}, Mo═O 937 cm^{-1}, Mo−F 480, 529 cm^{-1}. **$[C_6H_{18}N_2]_2[Mo_8Na_2O_{26}F_2(H_2O)_4] \cdot 4H_2O$ (7):** colorless blocks. Elem microanal. Obsd (calcd) for **7**: C, 10.55 (9.14); H, 3.20 (2.79); N, 4.05 (3.55); F, 2.50 (2.41). IR data: N−H 3118, 1579 cm^{-1}, C−H 1465 cm^{-1}, Mo═O 917 cm^{-1}, Mo−F 480, 529 cm^{-1}. **$[C_6H_{21}N_4]_2[Mo_8O_{26}F_2] \cdot 6H_2O$ (8):** colorless plates. Elem microanal. Obsd (calcd) for **8**: C, 8.97 (8.85); H, 3.86 (3.32); N, 7.65 (6.88); F, 2.40 (2.33). IR data: N−H 3124, 1604 cm^{-1}, C−H 1502 cm^{-1}, Mo═O 931 cm^{-1}. Powder X-ray diffraction patterns of each bulk sample match the pattern generated from the respective single-crystal X-ray structure. Deviations between the calculated and observed values of the carbon content in compounds **1**, **4**, and **7** are most likely the result of minor impurity phases that were not observed using powder diffraction.

Single-Crystal X-ray Diffraction. Data were collected using an Oxford Diffraction Xcalibur3 CCD diffractometer with enhanced Mo Kα radiation ($\lambda = 0.710\ 73$ Å). A single crystal was mounted on a glass fiber using *N*-paratone oil and cooled in situ to 110(2) K for data collection. Frames were collected, indexed, and processed and the files were scaled using *CrysAlis RED*.[30] The heavy-atom positions were determined using *SIR92*.[31] All other non-hydrogen sites were located from Fourier difference maps. All non-hydrogen sites were refined using anisotropic thermal parameters using full-matrix least-squares procedures on F_o^2 with $I > 3\sigma(I)$. Hydrogen atoms were placed in geometrically idealized positions. All calculations were performed using *Crystals*.[32] Relevant crystallographic data are listed in Table 1. Complete lists of crystallographic data are provided in CIF format in the Supporting Information.

Powder X-ray Diffraction. Powder X-ray diffraction patterns were recorded on a GBC-Difftech MMA powder diffractometer. Samples were mounted on aluminum plates. Calculated powder patterns were generated from single-crystal data using *ATOMS* version 6.0.[33]

Infrared Spectroscopy. Infrared measurements were obtained using a Perkin-Elmer FT-IR Spectrum 1000 spectrophotometer. Samples were diluted with spectroscopic-grade KBr and pressed into a pellet. Scans were run over the range of 400−4000 cm^{-1}.

Results

The inorganic components present in compounds **1**−**8** vary in dimensionality and connectivity; however, certain structural features are retained. Each second-order Jahn−Teller[3–5,34] active Mo^{VI} center exhibits a distorted octahedral geometry. $Mo-O_{terminal}$ bonds are generally shorter than $Mo-O_{bridging}$ bonds; the observed ranges are 1.693(4)−1.736(2) and 1.735(4)−2.4595(19) Å, respectively. A much wider spread in $Mo-O_{bridging}$ bonds is observed because the bridging oxides can be bound from anywhere between two and six adjacent molybdenum centers. Mo−F bond lengths range between 1.941(4) and 2.030(2) Å. Four distinct anion connectivities are observed: β-$[Mo_8O_{26}]^{4-}$ and $[Mo_8O_{26}F_2]^{6-}$ molecular anions and $[Mo_8O_{26}]_n^{4n-}$ and $[Mo_8O_{27}]_n^{6n-}$ chains.

***β*-$[Mo_8O_{26}]^{4-}$.** The well-known β-octamolybdate anion[27,35–38] is observed in **1** and **2**. These anions are constructed from eight $[MoO_6]$ octahedra that share common edges and vertices with one another to form the anions shown in Figure 1a.

$[Mo_8O_{26}]_n^{4n-}$. One-dimensional $[Mo_8O_{26}]_n^{4n-}$ chains[37,39] constructed from $[Mo_8O_{24}O_{4/2}]_n^{4n-}$ monomers are observed in **3**. These monomers are connected to one another through two shared corners. These chains are shown in Figure 2c.

$[Mo_8O_{27}]_n^{6n-}$. One-dimensional $[Mo_8O_{27}]_n^{6n-}$ chains[40] are observed in **4**. While these chains are constructed from the same monomer units present in $[Mo_8O_{26}]_n^{4n-}$, the mode of connection differs. Adjacent monomers in $[Mo_8O_{26}]_n^{4n-}$ are connected through two shared oxides, while neighboring $[Mo_8O_{27}]_n^{6n-}$ monomers share a lone oxide. These chains are shown in Figure 2e.

$[Mo_8O_{26}F_2]^{6-}$. Compounds **5**−**8** all contain $[Mo_8O_{26}F_2]^{6-}$ molecular anions.[41] These anions contain a γ-$[Mo_8O_{26}]^{4-}$-like core[42] to which two fluoride ligands have coordinated. See Figure 1b. The fluoride ligands are bound to the two five-coordinate molybdenum centers in γ-$[Mo_8O_{26}]^{4-}$.

Thermal ellipsoid plots and figures of the three-dimensional packing of compounds **1**−**8** are provided in the Supporting Information.

(30) *CrysAlis CCD and CrysAlis RED*, version 1.171; Oxford Diffraction Ltd.: Abdingdon, U.K., 2002.
(31) Altomare, A.; Cascarano, G.; Giacovazzo, C.; Guagliardi, A. *J. Appl. Crystallogr.* **1993**, *26*, 343–350.
(32) Betteridge, P. W.; Carruthers, J. R.; Cooper, R. I.; Prout, K.; Watkin, D. J. *J. Appl. Crystallogr.* **2003**, *36*, 1487.
(33) Dowty, E. *ATOMS*, version 6.0; Shape Software: Kingsport, TN, 2002.
(34) Halasyamani, P. S. *Chem. Mater.* **2004**, *16*, 3586–3592.
(35) Lindqvist, I. *Ark. Kemi* **1950**, *2*, 349–355.
(36) Harrison, W. T. A.; Stucky, G. D.; Gier, T. E. *Acta Crystallogr., Sect. C* **1993**, *C49*, 1900–1902.
(37) Nelson, J. H.; Johnston, A. R.; Narducci Sarjeant, A.; Norquist, A. J. *Solid State Sci.* **2007**, *9*, 472–484.
(38) Muller, E. A.; Sarjeant, A. N.; Norquist, A. J. *Acta Crystallogr., Sect. E* **2005**, *E61*, m730−m732.
(39) Xu, Y.; An, L.-H.; Koh, L.-L. *Chem. Mater.* **1996**, *8*, 814–818.
(40) Boeschen, I.; Buss, B.; Krebs, B. *Acta Crystallogr., Sect. B* **1974**, *30*, 48–56.
(41) Kamenar, B.; Kaitner, B.; Strukan, N. *Acta Crystallogr., Sect. C* **1990**, *C46*, 2249–2251.
(42) Niven, M. L.; Cruywagen, J. J.; Heyns, J. B. B. *J. Chem. Soc., Dalton Trans.* **1991**, 2007–2011.

Table 1. Crystallographic Data for Compounds **1**−**8**

	$[C_6H_{18}N_2]_2[Mo_8O_{26}]\cdot 2H_2O$ (**1**)	$[C_6H_{18}N_2]_2[Mo_8O_{26}]$ (**2**)	$[C_6H_{18}N_2]_2[Mo_8O_{26}]$ (**3**)	$[C_6H_{21}N_4]_2[Mo_8O_{27}]\cdot 2H_2O$ (**4**)
formula	$C_{12}H_{40}Mo_8N_4O_{28}$	$C_{12}H_{36}Mo_8N_4O_{26}$	$C_{12}H_{36}Mo_8N_4O_{26}$	$C_{12}H_{46}Mo_8N_8O_{29}$
fw	1455.98	1419.95	1419.95	1534.05
space group	$P\bar{1}$ (No. 2)	$P2_1/n$ (No. 14)	$P\bar{1}$ (No. 2)	$P\bar{1}$ (No. 2)
a/Å	7.8544(3)	8.9257(13)	9.0306(16)	9.525(3)
b/Å	10.7833(4)	15.717(2)	9.633(2)	10.239(4)
c/Å	11.3964(5)	11.9316(17)	10.538(3)	11.557(3)
α/deg	103.016(3)	90	104.13(2)	108.59(3)
β/deg	105.575(3)	97.862(12)	103.93(2)	110.34(3)
γ/deg	97.551(3)	90	95.297(17)	101.96(3)
V/Å^3	886.77(7)	1658.1(4)	851.6(4)	935.4(7)
Z	1	2	2	1
ρ_{calcd}/g cm^{-3}	2.726	2.844	2.769	2.723
λ/Å	0.710 73	0.710 73	0.710 73	0.710 73
T/K	110(2)	110(2)	110(2)	110(2)
μ/mm^{-1}	2.836	3.026	2.945	2.701
R1[a]	0.0231	0.0191	0.0265	0.0260
wR2[b]	0.0544	0.0466	0.0708	0.0489

	$[C_6H_{18}N_2]_3[Mo_8O_{26}F_2]\cdot 4H_2O$ (**5**)	$[C_6H_{18}N_2]_3[Mo_8O_{26}F_2]\cdot 5H_2O$ (**6**)	$[C_6H_{18}N_2]_2[Mo_8Na_2O_{26}F_2(H_2O)_4]\cdot 4H_2O$ (**7**)	$[C_6H_{21}N_4]_2[Mo_8O_{26}F_2]\cdot 6H_2O$ (**8**)
formula	$C_{18}H_{64}F_2Mo_8N_6O_{30}$	$C_{18}H_{64}F_2Mo_8N_6O_{31}$	$C_{12}H_{44}F_2Mo_8N_4Na_2O_{30}$	$C_{12}H_{54}F_2Mo_8N_8O_{32}$
fw	1648.23	1666.16	1575.99	1628.11
space group	$P\bar{1}$ (No. 2)	$P\bar{1}$ (No. 2)	$P2_1/c$ (No. 14)	$P\bar{1}$ (No. 2)
a/Å	10.2439(14)	12.0550(18)	11.4789(4)	9.707(3)
b/Å	10.8055(14)	13.9286(12)	15.9713(4)	10.571(3)
c/Å	21.380(3)	15.357(3)	11.9427(4)	12.1601(19)
α/deg	76.889(11)	76.302(12)	90	111.491(19)
β/deg	84.499(11)	83.388(15)	113.590(4)	103.33(2)
γ/deg	86.399(11)	70.958(10)	90	101.05(2)
V/Å^3	2292.2(5)	2366.1(7)	2006.52(12)	1075.9(5)
Z	2	2	2	1
ρ_{calcd}/g cm^{-3}	2.388	2.324	2.608	2.513
λ/Å	0.710 73	0.710 73	0.710 73	0.710 73
T/K	110(2)	110(2)	110(2)	110(2)
μ/mm^{-1}	2.220	2.153	2.547	2.367
R1[a]	0.0217	0.0337	0.0227	0.0207
wR2[b]	0.0547	0.0801	0.0687	0.0486

[a] $R1 = \sum||F_o| - |F_c||/\sum|F_o|$. [b] $wR2 = [\sum w(F_o^2 - F_c^2)^2/[\sum w(F_o^2)^2]^{1/2}$.

Distinguishing between oxide and fluoride ligands using diffraction data alone is difficult, owing to the similarities in their atomic scattering factors. For this reason, an analysis of the bond valence sums[43,44] of the $[Mo_8O_{26}F_2]^{6-}$ anions in **5**−**8** was performed. The bond length and valence ranges of the Mo−F bonds are appropriate for terminal fluoride bonds, 1.941(4)−2.030(2) Å and 0.55−0.70, respectively. However, these bonds are too long to be molybdenum oxide bonds because the total valences (0.72−0.91) would be unreasonably low. Additional support for these assignments is found in elemental analyses of the fluoride-containing compounds and infrared spectroscopy. $Mo-F_{terminal}$ stretches are clearly observed in the infrared spectra of compounds **5**−**8**.[45,46]

Discussion

Several reaction parameters have been directly addressed in order to improve our ability to synthesize new functional materials. First, understanding how the selection of specific polyoxomolybdate architectures can be achieved is paramount in the optimization of physical properties and requires a fundamental understanding of the variables that control speciation. Second, strategies for the elucidation of the correlations between organic amine and product structure are addressed on both a local and an extended scale. Third, the use of chiral organic amines is probed as a route to novel noncentrosymmetric compounds.

1. Polyoxomolybdate Structure. The chemistry of polyoxometalates has been studied extensively for several decades because of a host of desirable physical properties that compounds containing such anions can exhibit. The structural diversity of molybdenum-containing species has resulted in special attention to these anions; compounds containing inorganic components whose dimensionalities range between zero and three are common.[29,47,48] The speciation of molybdates is known to be pH-dependent, and it has been shown in aqueous reactions using electrospray mass spectrometry that mononuclear species predominate at low molybdate concentrations ($<10^{-4}$ M) and relatively high pH (∼6). The protonation of $[MoO_4]^{2-}$, the molybdate ion, begins at pH ≥7 and, as the reaction pH is decreased, proceeds through a

(43) Brown, I. D.; Altermatt, D. *Acta Crystallogr., Sect. B* **1985**, *B41*, 244–247.
(44) Brese, N. E.; O'Keeffe, M. *Acta Crystallogr., Sect. B* **1991**, *B47*, 192–197.
(45) Mattes, R.; Mennemann, K.; Jaeckel, N.; Rieskamp, H.; Brockmeyer, H. J. *J. Less Common Met.* **1980**, *76*, 199–212.
(46) Dirand, J.; Ricard, L.; Weiss, R. *Trans. Met. Chem.* **1976**, *1*, 2–5.
(47) Jiang, C.-C.; Liu, G.; Wei, Y.-G.; Wang, W.; Zhang, S.-W. *Inorg. Chem. Commun.* **1999**, *2*, 258–260.
(48) Hagrman, P. J.; Hagrman, D.; Zubieta, J. *Angew. Chem., Int. Ed.* **1999**, *38*, 2639–2684.

series of equilibrium steps.[49] The expansion of the Mo^{VI} coordination sphere from four to six likely governs the formation of polyanions from mononuclear species. $[Mo_7O_{24}]^{6-}$ is rapidly formed from the molybdate ion, suggesting an importance of $[Mo_7O_{24}]^{6-}$ in the formation of more complex polyanions. A reaction mechanism for the conversion of $[Mo_7O_{24}]^{6-}$ to β-$[Mo_8O_{26}]^{4-}$ has been proposed, based upon ^{17}O and ^{95}Mo NMR data. Rapid interconversion[50] of isomeric α- and β-$[Mo_8O_{26}]^{4-}$ species provides routes to larger polyanions.[51] In addition, the ability to precipitate minor molybdate species while the majority species remain in solution is known.

The hydrothermal chemistry of polyoxomolybdates involves many interrelated reaction variables, including the pH, the molybdenum source, the identities of other reaction species, the temperature, and time. In order to reduce the number of such variables and systematize the reactions, composition space analysis can be used.[8,52–54] Areas of selective crystallization, or "crystallization fields", are often observed. In order to isolate the effects of reaction gel variations from the pH, all reactions were adjusted to pH 5 before heating. Composition space diagrams for the MoO_3/$H_2N(CH_2)_5NH_2$/H_2O and MoO_3/$H_2N(CH_2)_7NH_2$/H_2O systems are shown in Figure 4. These two systems were selected to demonstrate how composition space analysis can be used to isolate multiple reaction variables in a given system and to explain complex phase stabilities.

The placement of the crystallization fields in MoO_3/$H_2N(CH_2)_5NH_2$/H_2O is dependent upon the compositions of the reaction products, specifically the relative Mo/amine ratios. Compounds containing $[Mo_3O_{10}]_n^{2n-}$ chains have a Mo/template ratio of 3:1, while compounds that contain any $[Mo_8O_{26}]^{4-}$ species have a Mo/template ratio of 4:1. It is observed that, in general, compounds containing $[Mo_3O_{10}]_n^{2n-}$ chains form under template-rich conditions, while $[Mo_5O_{16}]_n^{2n-}$ layers, $[Mo_8O_{26}]_n^{4n-}$ chains, and $[Mo_8O_{26}]^{4-}$ molecular anions form under Mo-rich conditions because, under these conditions, the reaction products have compositions that more closely match that of the reaction gel than other species.

This can be extended to include the effects of variation in the solvent concentration. The MoO_3/$H_2N(CH_2)_7NH_2$/H_2O system contains three compounds: $[C_7H_{20}N_2]_2[Mo_8O_{26}]$, $[C_7H_{20}N_2]_2[Mo_8O_{26}]\cdot H_2O$, and $[NH_4][Mo_6O_{18}]$. Unlike the MoO_3/$H_2N(CH_2)_5NH_2$/H_2O system described above, a strong dependence on the solvent water concentration between $[C_7H_{20}N_2]_2[Mo_8O_{26}]$ and $[C_7H_{20}N_2]_2[Mo_8O_{26}]\cdot H_2O$ is observed. $[C_7H_{20}N_2]_2[Mo_8O_{26}]$ is the dominant reaction product at lower to moderate water levels, while $[C_7H_{20}N_2]_2[Mo_8O_{26}]\cdot H_2O$ is observed at higher water concentrations. Again, the compound whose composition most closely mirrors that of the reaction gel is observed to be the dominant reaction product.

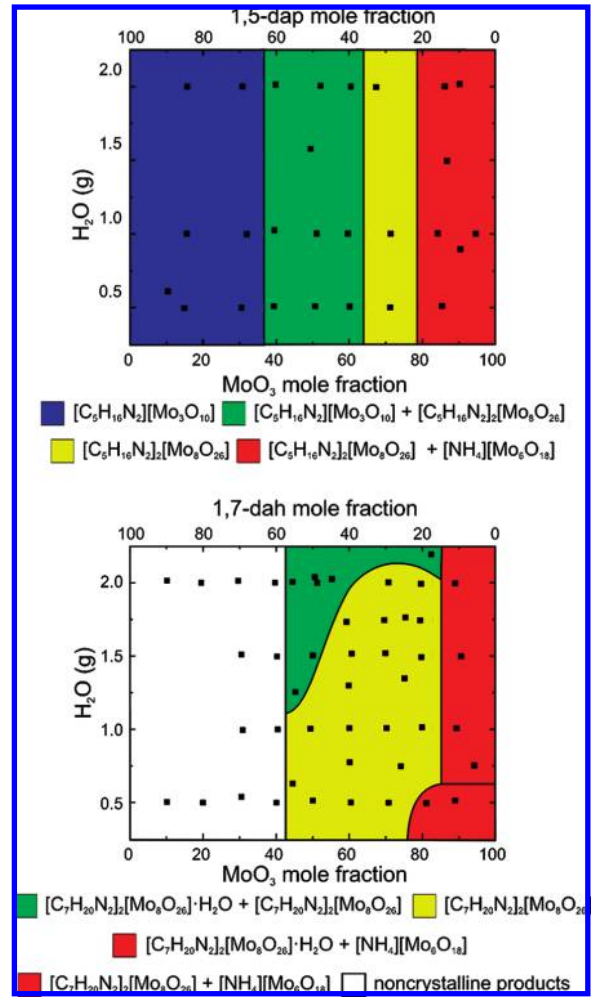

Figure 4. Composition space diagrams for the MoO_3/$H_2N(CH_2)_5NH_2$/H_2O and MoO_3/$H_2N(CH_2)_7NH_2$/H_2O systems.

2. Amine Structure. As noted by Ferey, amines can have profound roles in the formation of new inorganic materials.[55,56] It was proposed that charge density matching between the amine and inorganic component results in the formation of neutral ammonium−SBU pairs that then precipitate as solids. Therefore, the size, shape, and charge of the protonated organic amines play critical roles in the determination of the inorganic topology. Similar dependencies in molybdates were demonstrated through the precipitation of various polyoxoanions using a series of related amines ($[NH_4]^+$, $[(NH_2)_3C]^+$, $[(CH_3)_4N]^+$, and $[(C_4H_9)_4N]^+$).[57] One method for the elucidation of the effects associated with the amine structure is the use of a series of related amines.

Several groups have studied the synthesis of new materials using a series of related amines to determine how structural

(49) Walanda, D. K.; Burns, R. C.; Lawrance, G. A.; von Nagy-Felsobuki, E. I. *J. Chem. Soc., Dalton Trans.* **1999**, 311–322.
(50) Klemperer, W. G.; Shum, W. *J. Am. Chem. Soc.* **1976**, *98*, 8291–8293.
(51) Howarth, O. W.; Kelly, P.; Pettersson, L. *J. Chem. Soc., Dalton Trans.* **1990**, 81–84.
(52) Halasyamani, P.; Willis, M. J.; Stern, C. L.; Lundquist, P. M.; Wong, G. K.; Poeppelmeier, K. R. *Inorg. Chem.* **1996**, *35*, 1367–1371.
(53) Norquist, A. J.; Heier, K. R.; Stern, C. L.; Poeppelmeier, K. R. *Inorg. Chem.* **1998**, *37*, 6495–6501.
(54) Doran, M. B.; Norquist, A. J.; O'Hare, D. *Inorg. Chem.* **2003**, *42*, 6989–6995.
(55) Ferey, G. *J. Fluorine Chem.* **1995**, *72*, 187–193.
(56) Ferey, G. *Chem. Mater.* **2001**, *13*, 3084–3098.
(57) Himeno, S.; Niiya, N.; Ueda, T. *Bull. Chem. Soc. Jpn.* **1997**, *70*, 631–637.

changes affect the three-dimensional structure. It has been shown that the introduction of small changes into the template structure can have profound effects on the products in similar reactions. Examples include syntheses of zeolites,[58–60] uranium fluorides[61] and sulfates,[62,63] and gallium fluorophosphates.[55,64] Our investigations into the role of the amine in the formation of new polyoxomolybdates are focused on the effects of the amine structure and symmetry.

In our study of the $MoO_3/H_2N(CH_2)_nNH_2/H_2O$ ($n = 3-7$) systems,[37] a series of linear diamines was employed, with carbon backbone lengths ranging between 3 and 7. These amines are structurally similar, with consistent charges, hydrogen-bonding properties, and basicities across the series. It was observed using composition space analysis that a small set of molybdate species was present in many of the composition spaces. However, a direct comparison of the five composition space diagrams revealed several systematic differences.

It was observed that the range of the crystallization fields of $[Mo_3O_{10}]_n^{2n-}$-containing compounds was largest in the 1,3-dap system and decreased as the linear diamine chain length was increased. This mirrors the results reported by Himeno et al., who studied the solution stabilities of isopolymolybdates at different pHs in the presence of a series of related amines ($[NH_4]^+$, $[(CH_3)_4N]^+$, and $[(n\text{-}C_4H_9)_4N]^+$).[57] In reactions conducted between pH 4 and 6, it was found that smaller, higher-charge-density cations promote the formation of $[Mo_3O_{10}]_n^{2n-}$ chains and $[Mo_7O_{24}]^{6-}$ molecular anions, while α-$[Mo_8O_{26}]_n^{4n-}$ and β-$[Mo_8O_{26}]^{4-}$ are formed from solutions containing the larger cations. A decrease in the charge density is observed as the length of the linear diamine is increased, stabilizing compounds containing $[Mo_5O_{16}]_n^{2n-}$ layers, β-$[Mo_8O_{26}]^{4-}$ molecular anions, or $[Mo_8O_{26}]_n^{4n-}$ chains. In addition, decomposition of the amine was only observed in the 1,7-dah system, where there were no crystalline products in reactions where $\chi_{Mo} < 0.4$.

The inclusion of diamines that contain aromatic rings introduces additional structural changes. Two amines were studied, *p*-xylylenediamine[65] and 4-aminopyridine,[66,67] from which three compounds were synthesized. The ability of the amines to undergo $\pi-\pi$ stacking, which is absent from the linear diamines described above, promotes cation stacking, as is observed in the three-dimensional packings of $[C_5H_7N_2]_2[Mo_3O_{10}]$, $[C_5H_7N_2]_2[Mo_3O_{10}]$, and $[C_5H_{16}N_2]_2[Mo_8O_{26}]$. See Figure 5.

An additional series of reactions using deed, dmeed, tmed, or tren was conducted to probe the effects of differences in the cation charge and hydrogen-bonding properties with a series of structurally related amines. The relative mole fractions of each component were fixed; the only differences were the identities of the amines. When the pH, time, temperature, and relative reactant gel composition between experiments were fixed, direct observation of the effects introduced by the amine structure was possible. The four new compounds, denoted **1**−**4**, contain three different molybdate structures. Reactions using deed and dmeed resulted in compounds containing β-$[Mo_8O_{26}]^{4-}$, while the tmed and tren reactions resulted in $[Mo_8O_{26}]^{4-}$ type I and $[Mo_8O_{27}]_n^{6n-}$ chains, respectively.

Two distinct trends are observed in these reactions. First, the difference in charge between $[deedH_2]^{2+}$, $[dmeedH_2]^{2+}$, and $[tmedH_2]^{2+}$ with respect to $[trenH_3]^{3+}$ directly affects the form of the inorganic component in compound **4**. Compounds **1**−**3**, which contain $[deedH_2]^{2+}$, $[dmeedH_2]^{2+}$, and $[tmedH_2]^{2+}$ cations, respectively, contain two cations per

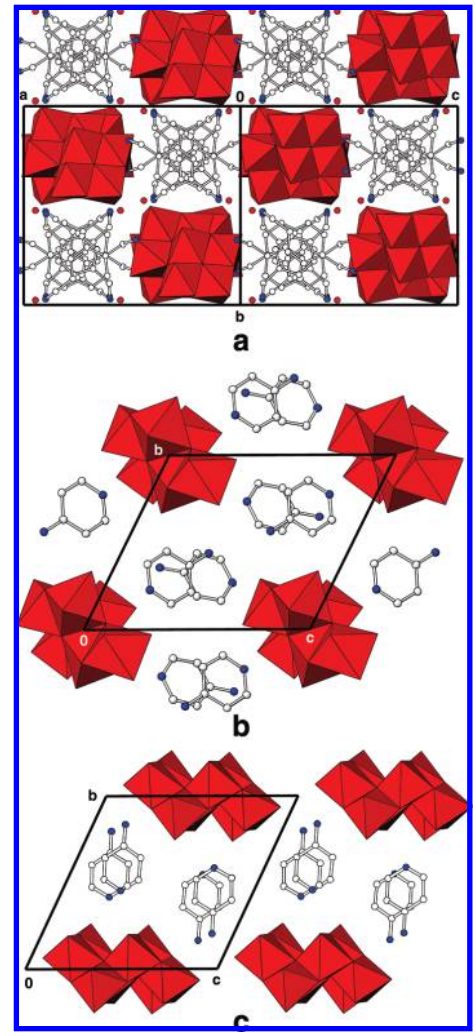

Figure 5. Three-dimensional packing diagrams of (a) $[C_8H_{14}N_2]_3[Mo_9O_{30}]\cdot 2H_2O$, (b) $[C_5H_7N_2]_2[Mo_3O_{10}]$, and (c) $[C_5H_7N_2]_4[Mo_8O_{26}]$. Red octahedra represent $[MoO_6]$, while white and blue circles represent carbon and nitrogen atoms, respectively. Hydrogen atoms have been removed for clarity.

(58) Tsuji, K.; Wagner, P.; Davis, M. E. *Microporous Mesoporous Mater.* **1999**, *28*, 461–469.
(59) Takewaki, T.; Beck, L. W.; Davis, M. E. *Microporous Mesoporous Mater.* **1999**, *33*, 197–207.
(60) Beck, L. W.; Davis, M. E. *Microporous Mesoporous Mater.* **1998**, *22*, 107–114.
(61) Francis, R. J.; Halasyamani, P. S.; Bee, J. S.; O'Hare, D. *J. Am. Chem. Soc.* **1999**, *121*, 1609–1610.
(62) Norquist, A. J.; Thomas, P. M.; Doran, M. B.; O'Hare, D. *Chem. Mater.* **2002**, *14*, 5179–5184.
(63) Norquist, A. J.; Doran, M. B.; O'Hare, D. *Solid State Sci.* **2003**, *5*, 1149–1158.
(64) Ferey, G.; Loiseau, T.; Lacorre, P.; Taulelle, F. *J. Solid State Chem.* **1993**, *105*, 179–190.
(65) Nelson, J. H.; Narducci Sarjeant, A.; Norquist, A. J. *Acta Crystallogr., Sect. E* **2007**, *E63*, m1442−m1444.
(66) Nelson, J. R.; Narducci Sarjeant, A.; Norquist, A. J. *Acta Crystallogr., Sect. E* **2006**, *E62*, m1731−m1733.
(67) Nelson, J. R.; Narducci Sarjeant, A.; Norquist, A. J. *Acta Crystallogr., Sect. E* **2006**, *E62*, m1448−m1450.

β-$[Mo_8O_{26}]^{4-}$ molecular anion or $[Mo_8O_{26}]_n^{4n-}$ chain monomer. Compound **4** contains the same 2:1 ratio of amines to anion formula unit. However, in order to compensate for the additional charge on the $[trenH_3]^{3+}$ cations, a different chain type is observed. While $[Mo_8O_{27}]_n^{6n-}$ chains are constructed from the same γ-$[Mo_8O_{26}]^{4-}$-type building units[42] as $[Mo_8O_{26}]_n^{4n-}$ type I and II chains, a reduction in the number of shared oxides between monomers results in an increased charge to compensate for $[trenH_3]^{3+}$ cations. Second, two distinct molybdate anion types are observed in compounds **1**−**3**, which contain the three amines with the most closely related structures. $[deedH_2]^{2+}$, $[dmeedH_2]^{2+}$, and $[tmedH_2]^{2+}$ cations all share the same charge and formula. However, their hydrogen-bonding properties and associated steric constraints differ dramatically. Both $[deedH_2]^{2+}$ and $[dmeedH_2]^{2+}$ contain secondary amines, each of which can donate two hydrogen bonds, while $[tmedH_2]^{2+}$ only contains tertiary amines. $[tmedH_2]^{2+}$ cations are essentially flat and require a single hydrogen-bond acceptor both above and below the plane of the cation. This is achieved in **3** by a packing motif in which $[tmedH_2]^{2+}$ cations lie parallel to two adjacent $[Mo_8O_{26}]_n^{4n-}$ chains and donate a single hydrogen bond to each. Such packing is not possible using $[deedH_2]^{2+}$ and $[dmeedH_2]^{2+}$ cations because the steric constraints are different. The $[deedH_2]^{2+}$ and $[dmeedH_2]^{2+}$ cations in **1** and **2** both contain secondary amines and require multiple acceptors to be close to each nitrogen center along the H−N−H bond angles, cannot adopt the same packing motif present in **3**, and do not favor the formation of $[Mo_8O_{26}]_n^{4n-}$ chains over β-$[Mo_8O_{26}]^{4-}$ molecular anions.

As stated above, the ability of octamolybdates to transform into other polyoxomolybdate species is well-known, many of which contain the important intermediate γ-$[Mo_8O_{26}]^{4-}$. This anion has been observed as a secondary building unit in the extended structures of several other compounds. The structure-directing properties of γ-$[Mo_8O_{26}]^{4-}$ are known to be dictated by the internal bonding motifs present.[27,68,69] The presence of two five-coordinate molybdenum centers in γ-$[Mo_8O_{26}]^{4-}$ causes substantial overbonding in selected bridging oxides,[70] and subsequent coordination is directed through these two molybdenum sites to relieve these bond stresses, as observed in $[Mo_8O_{26}]_n^{4n-}$[39,71] and $[Mo_8O_{27}]_n^{6n-}$ chains[40] and $[Mo_8O_{26}F_2]^{6-}$[41] and $[Mo_{16}O_{53}F_2]^{12-}$ molecular anions.[72]

Attack at the five-coordinate molybdenum centers often leads to polymeric structures that are constructed from γ-$[Mo_8O_{26}]^{4-}$-like monomer units and connected via oxide bridges. See Figure 2c−e. In contrast, the presence of fluoride in such reactions tends to result in the formation of molecular anions because of the difference in the bonding properties of oxide and fluoride. These Mo−O and Mo−F bonds have lengths that typically range from 1.83 to 1.93 Å and from 1.94 to 2.03 Å, respectively. The valences of the Mo−O bonds, 0.9−1.2, are appropriate in magnitude to allow the oxides to bridge between neighboring molybdenum centers, while the Mo−F valences in $[Mo_8O_{26}F_2]^{6-}$, 0.6−0.7, are sufficiently high to preclude Mo−F−Mo bridges.

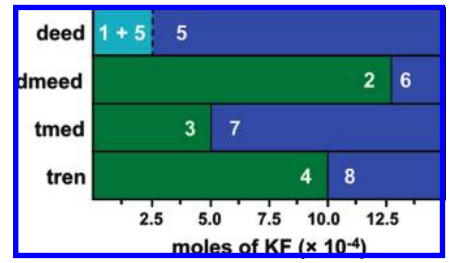

Figure 6. Plot of the product composition as a function of the number of moles of KF in the $Na_2MoO_4 \cdot 2H_2O$/amine/H_2O/KF systems (amine = deed, dmeed, tmed, and tren).

In order to directly compare the fluoride and amine structures, a series of experiments with approximate compositions of 1.5:1:100:1.25:*x* $Na_2MoO_4 \cdot 2H_2O$:amine:H_2O:H_2SO_4:KF (amine = deed, dmeed, tmed, and tren; x = 0−0.8) was conducted. The results of these reactions are plotted in Figure 6.

Reactions conducted in the absence of KF produced compounds **1**−**4**. Four additional compounds, one for each of the amines studied, were synthesized from reactions containing KF. The great diversity in the molybdate structure observed in compounds **1** −**4** was absent from compounds **5**−**8**, which all contain the same $[Mo_8O_{26}F_2]^{6-}$ molecular anions. See Figure 1b. If sufficient F^- is present, the role of the amine is diminished and the final molybdate structure is defined by the action of the fluoride. In the absence of F^-, the role of the amine exerts considerable importance and stark differences in the molybdate structure are observed for analogous reactions conducted at the same temperature and pH.

The amount of KF required for the synthesis of these new compounds, denoted **5**−**8**, varied between amine systems. **5** was observed in reactions conducted at the lowest KF levels (x = 0.2). In contrast, **6** did not form until much higher KF concentrations (x = 0.8). **7** and **8** were each observed at intermediate KF concentrations, x = 0.6 and 0.75, respectively. It is noted that compounds **5** and **7** contain symmetrical amines (deed and tmed) and are observed at low [F^-], while compounds **6** and **8** contain asymmetrical amines (dmeed and tren) and are only observed at higher [F^-]. This is most likely a result of packing differences associated with the different organic amines.

3. Amine Symmetry. In order to promote the formation of new noncentrosymmetric compounds, we have studied the use of chiral organic amines under different reaction conditions. Two systems have been investigated, MoO_3/3-aminoquinuclidine/H_2O/H_2SO_4 and MoO_3/2-methylpiperazine/H_2O/H_2SO_4, from which four new noncentrosymmetric compounds have been synthesized.[25−27]

In the MoO_3/3-aminoquinuclidine/H_2O/H_2SO_4 system,[27] reaction conditions were optimized through the construction of a composition space diagram using racemic 3-aminoquinuclidine. The initial pH of these reactions was adjusted to

(68) Heier, K. R.; Norquist, A. J.; Wilson, C. G.; Stern, C. L.; Poeppelmeier, K. R. *Inorg. Chem.* **1998**, *37*, 76–80.
(69) Maggard, P. A.; Nault, T. S.; Stern, C. L.; Poeppelmeier, K. R. *J. Solid State Chem.* **2003**, *175*, 27–33.
(70) Bridgeman, A. J. *J. Phys. Chem. A* **2002**, *106*, 12151–12160.
(71) Chakrabarti, S.; Natarajan, S. *Cryst. Growth Des.* **2002**, *2*, 333–335.
(72) Stover, A. K.; Gutnick, J. R.; Narducci Sarjeant, A.; Norquist, A. J. *Inorg. Chem.* **2007**, *46*, 4389–4391.

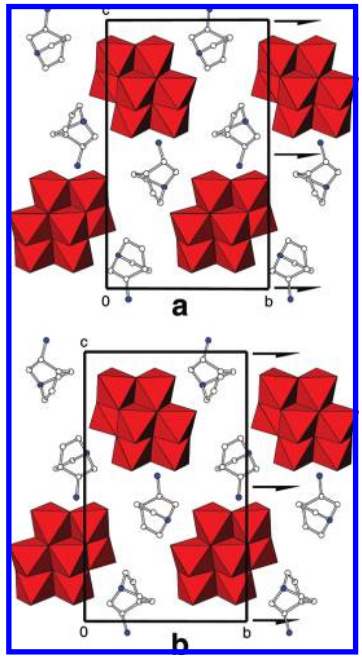

Figure 7. Three-dimensional packing diagrams of (a) [(*R*)-$C_7H_{16}N_2]_2[Mo_8O_{26}]$ and (b) [(*S*)-$C_7H_{16}N_2]_2[Mo_8O_{26}]$. Red octahedra represent [MoO_6], while white and blue circles represent carbon and nitrogen atoms, respectively. The symmetry elements present are shown. Hydrogen atoms have been removed for clarity.

5. Three compounds were synthesized, each of which was centrosymmetric and contained both (*R*)- and (*S*)-3-aminoquinuclidine in the structures. Reactions using enantiomorphically pure 3-aminoquinuclidine resulted in the formation of two new compounds that crystallize in the noncentrosymmetric space group $P2_1$ (No. 4), [(*R*)-$C_7H_{16}N_2]_2[Mo_8O_{26}]$ and [(*S*)-$C_7H_{16}N_2]_2[Mo_8O_{26}]$. The use of enantiomerically pure sources of chiral organic amines in the syntheses of [(*R*)-$C_7H_{16}N_2]_2[Mo_8O_{26}]$ and [(*S*)-$C_7H_{16}N_2]_2[Mo_8O_{26}]$ precludes the formation of the centers of inversion that were observed in $[C_7H_{16}N_2]_2[Mo_8O_{26}]\cdot H_2O$, $[C_7H_{16}N_2][Mo_3O_{10}]\cdot H_2O$, or $[C_7H_{16}N_2]_2[Mo_8O_{26}]\cdot 4H_2O$. The relationship of a [(*R*)-$aqnH_2]^{2+}$ cation through an inversion center to an adjacent [(*S*)-$aqnH_2]^{2+}$ cation is not possible because the presence or absence of these enantiomers is chemically controlled; no [(*S*)-$aqnH_2]^{2+}$ cations can be incorporated into the resulting solid if [(*R*)-$aqnH_2]^{2+}$ cations alone are present in the reaction gel. This constrains the space group of the solid to be noncentrosymmetric. The chirality of the [(*R*)-$aqnH_2]^{2+}$ and [(*S*)-$aqnH_2]^{2+}$ cations is reflected in the enantiomorphic and polar crystal class of these two compounds, 2 (C_2). A packing diagram of these two compounds is shown in Figure 7, with symmetry elements shown.

[(*S*)-$C_5H_{14}N_2][(MoO_3)_3(SO_4)]\cdot H_2O$[26] and [(*R*)-$C_5H_{14}N_2$]-$[(MoO_3)_3(SO_4)]\cdot H_2O$[25] were synthesized from the MoO_3/2-methylpiperazine/H_2O/H_2SO_4 system, from reactions in which the initial pH was adjusted to 2. Each compound crystallizes in the noncentrosymmetric space group $P2_12_12_1$ (No. 19). See Figure 8. While the form of the inorganic component in these two reactions differs greatly from the 3-aminoquinuclidine work, the result of crystallographic noncentrosymmetry remains the same. The presence or absence of each 2-methylpiperazine enantiomer is chemically

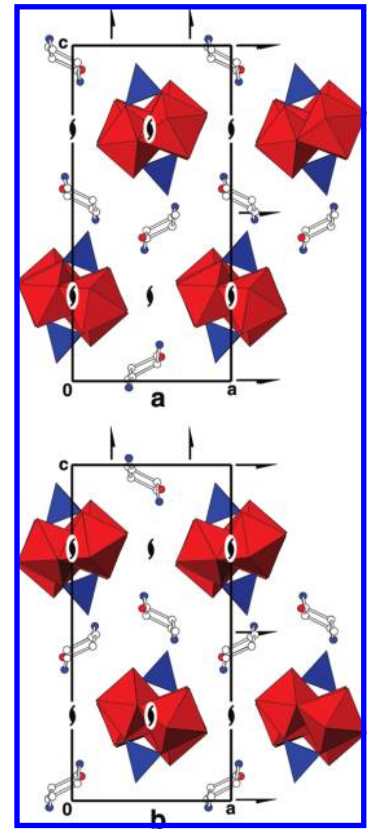

Figure 8. Three-dimensional packing diagrams of (a) [(*S*)-$C_5H_{14}N_2][(MoO_3)_3(SO_4)]\cdot H_2O$ and (b) [(*R*)-$C_5H_{14}N_2][(MoO_3)_3(SO_4)]\cdot H_2O$. Red and octahedra represent [MoO_6] and [SO_4], respectively. White, red, and blue circles represent carbon, oxygen, and nitrogen atoms, respectively. The symmetry elements present are shown. Hydrogen atoms have been removed for clarity.

controlled. The inclusion of only [(*R*)-$C_5H_{14}N_2]^{2+}$ cations in [(*R*)-$C_5H_{14}N_2][(MoO_3)_3(SO_4)]\cdot H_2O$ forces crystallization in a noncentrosymmetric space group because no [(*S*)-$C_5H_{14}N_2]^{2+}$ cations are present.

Conclusion

Understanding the factors that govern product composition and the role of the organic amine structure and symmetry can lead to control of the hydrothermal reaction products and the rational design of new functional materials. This was accomplished through the combination of composition space analysis and the use of a series of related organic amines.

Acknowledgment is made to the donors of the American Chemical Society, Petroleum Research Fund, and to the Research Corporation and the Howard Hughes Medical Institute for support. A.N.S. gratefully acknowledges support from the National Science Foundation (Award CHE-0215963).

Supporting Information Available: X-ray crystallographic file containing complete tables of atomic coordinates, thermal parameters, and bond lengths and angles (CIF), specific reaction descriptions, three-dimensional packing diagrams, thermal ellipsoid plots, and tables of bond valence sums for **1**−**8**. This material is available free of charge via the Internet at http://pubs.acs.org.

IC800572G